# Light Trapping in Thin Crystalline Si Solar Cells Using Surface Mie Scatterers

Pierpaolo Spinelli and Albert Polman

***Abstract*—Dielectric nanoparticles placed on top of a thin-film solar cell strongly enhance light absorption in the cell over a broad spectral range due to the preferential forward scattering of light from leaky Mie resonances in the particle. In this study, we systematically study with numerical simulations the absorption of light into thin (1–100 $\mu$m) crystalline Si solar cells patterned with Si nanocylinder arrays on top of the cell. We then use an analytical model to calculate the solar cell efficiency, based on the simulated absorption spectra. Using realistic values for bulk and surface recombination rates, we find that a 20-$\mu$m-thick Si solar cell with 21.5% efficiency can be made by using the Si nanocylinder Mie coating.**

***Index Terms*—Nanophotonics, silicon, solar cells.**

## I. Introduction

CRYSTALLINE Si (c-Si) is currently the most widely used semiconductor for photovoltaics applications. Despite continued technological developments that bring down the production costs of c-Si solar cells, the intrinsic Si material costs in these cells still remain high. For this reason, making thinner c-Si solar cells in order to use less of this expensive material continues to be a main driving force for the photovoltaic research community. Recent technological advances have led to the fabrication of thin-film c-Si solar cells on glass substrates by liquid phase crystallization [1]–[3] and layer transfer [4], [5]. However, thinner c-Si solar cells do not fully absorb the incoming light, especially in the near-bandgap spectral range, where the absorption length of Si exceeds the thickness of the cell. Light trapping is thus needed in order to achieve complete absorption of light in the cell.

Standard c-Si solar cells usually have a thickness of around 180 $\mu$m. At the front side, they are covered with a pyramidal light-trapping texture coated with an 80-nm-thick $Si_3N_4$ antireflection layer [6]. The typical feature size of the texturing is in the range 5–10 $\mu$m [7]. Therefore, it is impossible to apply this light-trapping texture to thinner cells with thicknesses in the micrometer range. Recently, metal and dielectric nanostructures have been considered as light-trapping coatings for ultrathin solar cells [8]–[14]. We have shown that an array of dielectric nanoparticles placed on top of Si wafer acts as an efficient antireflection coating [15]. This is due to the preferential scattering of light toward the high index substrate from leaky Mie resonances that are excited in the nanoparticles [16], [17]. In particular, we have shown that an optimized array of Si nanocylinders (NCs) yields broadband and omnidirectional ultralow reflectivity, reducing the reflection of a Si wafer to an average value as small as 1.3% [15].

In this paper, we investigate the potential of these Mie resonator coatings for light trapping in thin (1–100 $\mu$m) Si solar cells. Using numerical methods, we systematically study light absorption into thin Si slabs patterned with dielectric nanoparticle arrays with different geometries on top of the slab. We use finite-difference time domain (FDTD) simulations (employing periodic boundary conditions) to calculate light absorption of the c-Si slabs and compare it with that of a flat Si slab with a standard $Si_3N_4$ antireflection coating. An analytical model is then used to calculate, based on the simulated absorption spectra, the photocurrent, open-circuit voltage, and the efficiency of a c-Si solar cell with a Mie scattering surface coating and a metallic back contact. The model includes Shockley–Read–Hall bulk carrier recombination, surface recombination, and radiative and Auger recombination. Using realistic values for the recombination rates and a perfectly reflecting back contact, we find that an efficiency as high as 21.5% can be achieved for a 20-$\mu$m-thick cell with a Si NC Mie coating. This is a significant improvement compared with the efficiency that we find for a planar c-Si cell with a standard $Si_3N_4$ antireflection coating of the same thickness (17.5%). We also investigate the effect of an absorbing Ag back contact on the efficiency.

## II. Simulation Results

We use FDTD simulations [18] to calculate the absorption of light in thin Si slabs covered with square arrays of Si NC Mie scatterers, for wavelengths in the range 300–1150 nm. The Si NC coating is comprised of 250-nm-wide, 150-nm-high Si cylinders in an array with 450-nm pitch, conformally coated with a 50-nm-thick $Si_3N_4$ layer. These parameters are optimized for minimizing the reflection of a bulk Si wafer with a Si NC coating [15]. We use a cylindrical nanoparticle shape as it reduces the computational power needed for the simulations. However, a tapered-cylinder shape could be easier to fabricate and coat from a technological point of view. We have verified that tapering the NCs by an angle up to 20° does not significantly affect their optical scattering properties. A perfect reflector is applied at the

Manuscript received August 16, 2013; revised October 10, 2013 and November 11, 2013; accepted November 18, 2013. This work is a part of the research program of the Foundation for Fundamental Research on Matter, supported by the Netherlands Organization for Fundamental Research. It is also funded by the European Research Council. This work is also part of the Global Climate and Energy Project.

The authors are with the Center for Nanophotonics, FOM Institute AMOLF 1098 XG Amsterdam, The Netherlands (e-mail: spinelli@amolf.nl; polman@amolf.nl).

Color versions of one or more of the figures in this paper are available online at http://ieeexplore.ieee.org.

Digital Object Identifier 10.1109/JPHOTOV.2013.2292744

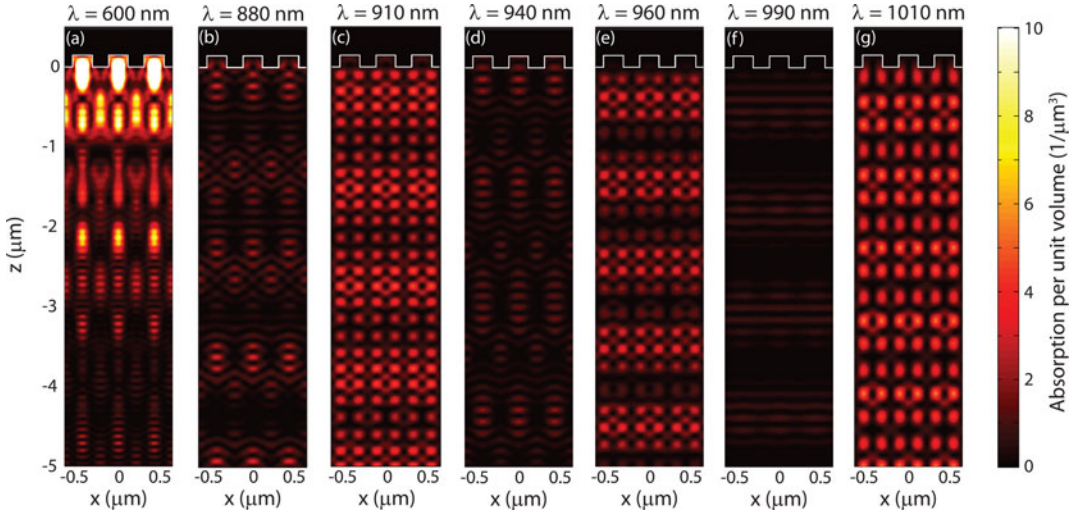


Fig. 1. Numerically calculated absorption per unit volume (color scale) in a vertical cross section of a 5-$\mu$m-thick Si slab with the Si NC Mie coating. Each panel represents a different wavelength and shows three horizontal unit cells. The absorption of light takes place according to complicated patterns determined by interference of the light scattered by the NCs.

back of the Si slab, and periodic boundary conditions are used. The absorption in both the Si slab and the Si NCs is calculated, as well as the reflection.

Fig. 1 shows the absorption per unit volume (color scale) in a vertical cross section of a 5-$\mu$m-thick Si slab coated with the Si NC Mie coating. Each panel shows the absorption profile for a different wavelength, in the range $\lambda = 600$–$1010$ nm. The white contours in the top part of each plot indicate the position of the Si NCs; three horizontal unit cells are shown in each panel. As can be seen, the absorption profiles inside the thin Si slab have complex patterns, which vary for different wavelengths. The patterns result from the interference of light scattered by the NC array in combination with reflection from the back surface. Fig. 1(a) shows that in the visible spectral range (e.g., $\lambda = 600$ nm), the absorption of light occurs mostly inside the Si NC and in the top part of the Si slab. The absorption patterns in the near-infrared spectral range are strongly dependent on the wavelength. For wavelengths of 880, 940, and 990 nm [see Fig. 1(b), (d), and (f)], the absorption is rather weak, whereas for wavelengths of 910, 960, and 1010 nm [see Fig. 1(c), (e), and (g)], the absorption profiles show bright absorption spots with a double periodicity with respect to an array pitch. We attribute these absorption profiles to the complex interplay of light coupled to Fabry–Perot and waveguide modes in the thin slab [19]. The plots in Fig. 1 can be used to calculate the total absorption in the Si slab and in the Si NCs by integrating the absorption per unit volume over the volume of the slab and the NCs, respectively.

Fig. 2 shows the combined absorption in Si slab and Si NCs as a function of wavelength for the patterned slab (red), compared with that for a flat Si slab with a standard 80 nm $Si_3N_4$ coating (blue). Data are shown for (a) 5-$\mu$m-thick and (b) 20-$\mu$m-thick Si slabs. The graphs show that absorption is enhanced over the entire 300–1100 nm spectral range by the presence of the Mie nanoscatterers on the front surface. This can be explained by two main mechanisms. First, the Mie scatterers provide an

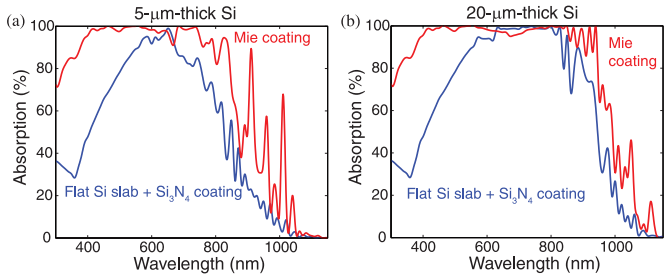


Fig. 2. Simulated absorption spectra for (a) a 5-$\mu$m-thick and (b) a 20-$\mu$m-thick Si slab with (red) and without (blue) a surface coating of Si nanocylinders. Absorption in the particles and in the Si slab are both taken into account. The flat and patterned geometries are coated with 80-nm and 50-nm-thick $Si_3N_4$ coatings, respectively. The absorption of the slab with Mie coating is larger than the standard coating over the entire spectral range. This is due to an improved antireflection effect and to light coupling to waveguide modes of the thin slabs.

antireflection effect, due to the preferential forward scattering toward the Si slab as we demonstrated earlier for thick Si wafers [15]. This effect improves the absorption over a broad spectral range from the ultraviolet to the near infrared. Second, the array of Mie scatterers couples the incoming light to waveguide modes in the thin Si slab. This effect is responsible for the absorption enhancement in the near-infrared spectral range. The main sharp peaks at 910, 960, and 1100 nm for the 5-$\mu$m-thick slab with the Mie coating (in red; see also absorption profiles in Fig. 1) are ascribed to coupling to Fabry–Perot and waveguide modes by the Mie resonances in the Si NC [19]. These main peaks are not observed for the flat reference. The smaller oscillations in the absorption spectrum of both the Mie-coated sample and the flat slab (blue) are due to Fabry–Perot interferences in the Si/$Si_3N_4$ layer stack, as can be derived from their free spectral range. For the 20-$\mu$m-thick slab, a broad enhancement is observed above $\lambda = 900$ nm, on top of the Fabry–Perot resonances, which we ascribe to coupling to a quasi-continuum of waveguide modes; for this large thickness, individual waveguide-coupling peaks

cannot be spectrally separated due to the high density of modes in the waveguide.

The absorption data shown in Fig. 2 can be used to calculate the total photocurrent generated in the thin Si cell. Note that the absorption spectra in Fig. 2 include the absorption in the Si NCs; this is a valid assumption if a junction can be made that is conformal to the nanoparticles or for solar cells where the junction is placed at the back. For a standard diffused homojunction design, the absorption in the NPs must be considered as a parasitic loss. First, a uniform photocarrier generation rate is assumed throughout the thickness of the Si slab. In practice, this means that the absorption profiles shown in Fig. 1 are averaged out over the volume of the slab. This is a valid assumption for crystalline Si, for which the carrier diffusion length is larger than the thickness of the solar cell considered in this study. The generation rate $G$ per unit volume can be calculated by

$$G = \frac{1}{t}\int_{\lambda} \frac{\lambda}{hc} I(\lambda) A(\lambda) d\lambda \tag{1}$$

where $t$ is the Si slab thickness, $I(\lambda)$ is the AM1.5g solar power spectrum, $A(\lambda)$ is the simulated absorption spectrum, $h$ is Planck's constant, and $c$ the speed of light. Assuming the slab is made of n-type Si, the generation rate $G$ is then used in the diffusion equation for holes in the quasi-neutral region [6]:

$$D_h \frac{d^2 \Delta p}{dx^2} = \frac{\Delta p}{\tau_b} - G \tag{2}$$

where $D_h$ is the minority carrier diffusion constant, $\Delta p$ is the excess hole concentration, $\tau_b$ is the bulk lifetime for holes, and $x$ the position across the thickness of the cell. Equation (2) can be solved assuming the boundary conditions

$$\Delta p\,|_{x=0} = \frac{n_i^2}{N_D}\left(e^{\frac{qV}{kT}} - 1\right) \text{ and } \left.\frac{d\Delta p}{dx}\right|_{x=t} = -\frac{S}{D_h}\Delta p(t) \tag{3}$$

where $N_D$ is the doping level, $V$ the voltage across the cell, $n_i$ is the intrinsic carrier concentration, and $S$ the back surface recombination rate. An infinitely thin p-n junction is assumed at the front surface ($x = 0$). Realistic devices that come close to this approximation are, e.g., heterojunction a-Si/c-Si solar cells, where the a-Si emitter is only a few nanometers thick [20]. For these cells, however, parasitic absorption in the thin a-Si layer must be taken into account. Solving equation (2) for $\Delta p$ and calculating the current density as $J = -qD_h \frac{d\Delta p}{dx}$ yields the solution for $J(V)$ as follows:

$$J = j_0\left(e^{\frac{qV}{kT}} - 1\right) - q\mathrm{LG}\left(\frac{L}{L_{j0}} - \frac{\mathrm{LS}}{F}\right) \tag{4}$$

with

$$L = \sqrt{\tau_b D_h}$$

$$L_{j0} = L\frac{D_h \cosh(x) + \mathrm{SL}\sinh(x)}{\mathrm{SL}\cosh(x) + D_h \sinh(x)}$$

$$j_0 = \frac{qD_h n_i^2}{L_{j0} N_D}$$

$$F = D_h \cosh(x) + \mathrm{SL}\sinh(x)$$

which is in agreement with [21], for the case of uniform carrier generation rate. Equation (4) represents the *J–V* characteristic of the solar cell that is based on the aforementioned assumptions. The short-circuit current density $J_{\mathrm{SC}}$, the open-circuit voltage $V_{\mathrm{OC}}$, the fill factor, and efficiency $\eta$ are easily calculated from this relation.

The free parameters in the model are the bulk lifetime $\tau_b$, the surface recombination velocity *S,* and doping level $N_D$. The bulk lifetime $\tau_b$ can be written as

$$\frac{1}{\tau_b} = \frac{1}{\tau_{\mathrm{SRH}}} + \frac{1}{\tau_{\mathrm{Auger}}} + \frac{1}{\tau_{\mathrm{rad}}} \tag{5}$$

where $\tau_{\mathrm{SRH}}$ lifetime representing Shockley–Read–Hall bulk recombination, $\tau_{Auger}$ is the lifetime representing Auger recombination, and $\tau_{rad}$ is the radiative recombination lifetime. For n-type Si, a semiempirical expression for (5) is [22]

$$\frac{1}{\tau_b} = \frac{1}{\tau_{\mathrm{SRH}}} + (N_D + \Delta n)(1.8 \times 10^{-24} N_D + 3 \times 10^{-27}\Delta n + \\ + 9.5 \times 10^{-15}) \quad \left(N_D,\ \Delta n \text{ in units of cm}^{-3},\ \tau \text{ in s}\right) \tag{6}$$

where $\Delta n$ is the injected carrier concentration, which is directly related to the open-circuit voltage $V_{\mathrm{OC}}$, as shown in [23]. The set of (4)–(6) can be solved recursively. In the following, we assume a fixed $N_D = 10^{16}$ cm$^{-3}$, and $\tau_{\mathrm{SRH}}$ and $S$ are varied.

Fig. 3 shows calculations of $J_{\mathrm{SC}}$ panels (a), (d), (g), $V_{\mathrm{OC}}$ (b), (e), (h), and efficiency (c), (f), (i) as a function of Si slab thickness. The top row assumes $\tau_{\mathrm{SRH}} = 1$ ms and $S = 10$ cm/s (good bulk material quality and surface passivation), the middle row $\tau_{\mathrm{SRH}} = 1$ ms and $S = 100$ cm/s (good material quality and poor surface passivation) and the bottom row $\tau_{\mathrm{SRH}} = 0.1$ ms and $S = 10$ cm/s (poor material quality and good surface passivation). Each panel shows data for a Si slab with a standard 80-nm $Si_3N_4$ coating (blue) and for a Si slab with a Mie coating (in red; same Si NC geometry as in Fig. 2). The latter is calculated considering absorption spectra that include both the absorption in the Si slab and absorption in the Si NCs at the surface. For reference, Fig. 3 also shows data for a Si slab with a perfect antireflection coating and a perfect Lambertian light-trapping surface, where the (geometrical) path length enhancement at long wavelengths equals $4n^2$, with $n$ the refractive index of Si (black-dashed lines) [24], [25]. Note that this implementation of the $4n^2$ limit is valid only in the low absorption regime, i.e., for very thin Si slabs. The actual limit is thus lower than the Lambertian limit for thicker c-Si slabs.

Fig. 3(a) shows that the photocurrent is strongly enhanced for all thicknesses due to the surface Mie scatterers. The photocurrent enhancement is more significant for thicknesses below 20 $\mu$m, where the Mie scatterers provide both an antireflection effect and strong light trapping due to coupling to waveguide modes in the thin Si slab. For a 1-$\mu$m-thick cell, the photocurrent is enhanced by as much as 75% due to the Si Mie coating for a large part due to light trapping. For a 20-$\mu$m-thick cell, a photocurrent enhancement of 20% is observed. For thicknesses above 20 $\mu$m, the photocurrent enhancement converges to the same value for all cell thickness, as the light-trapping effect

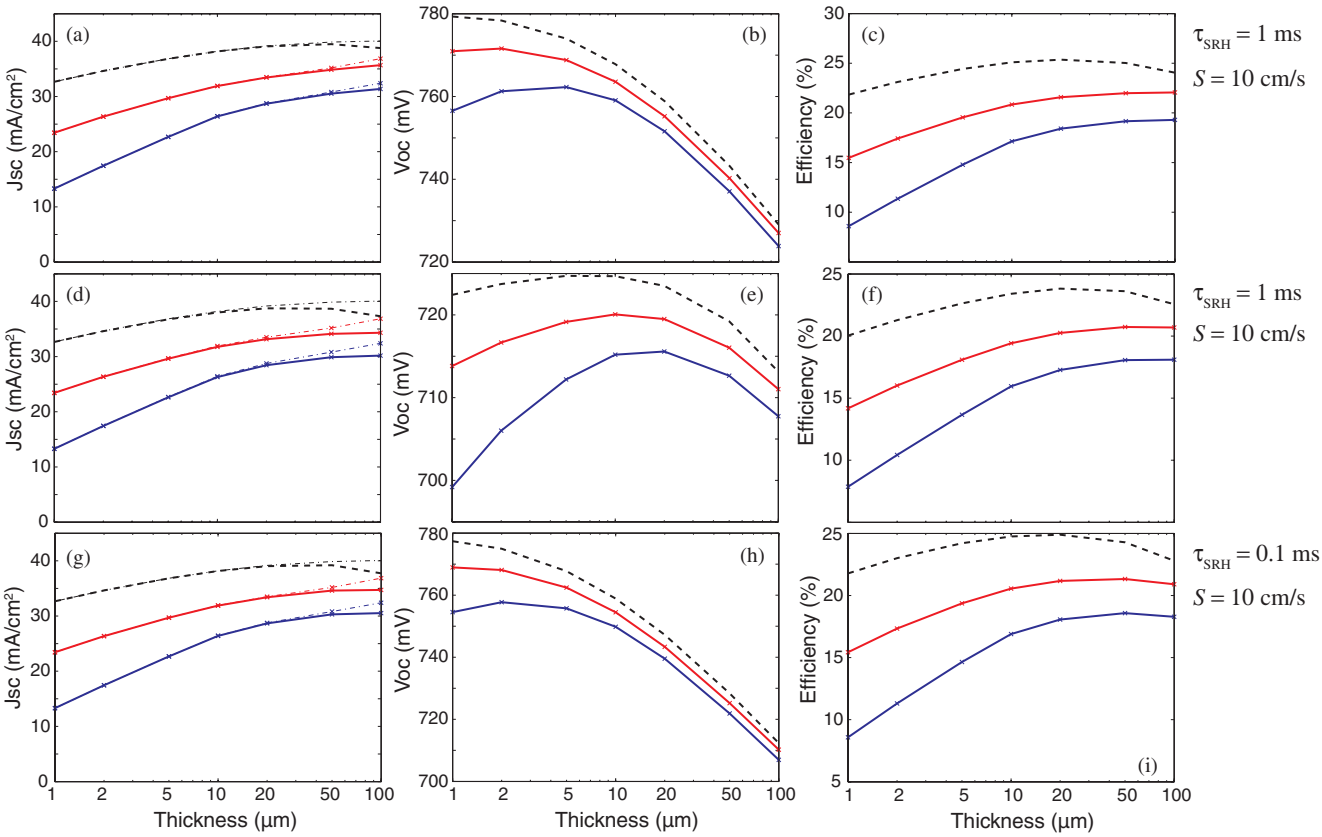


Fig. 3. Simulated short-circuit current density [(a), (d), (g)] open-circuit voltage, [(b), (e), (h)], and efficiency [(c), (f), (i)] as a function of Si layer thickness. Top panels assume $\tau_{\rm SRH} = 1$ ms and $S = 10$ cm/s, center panels $\tau_{\rm SRH} = 1$ ms and $S = 100$ cm/s, and bottom panels $\tau_{\rm SRH} = 0.1$ ms and $S = 10$ cm/s. In each panel, data for a slab with Mie scatterers (red) and a flat Si slab with standard $Si_3N_4$ coating (blue) are shown. The data for an ideal cell without reflection and with light trapping according to the geometrical $4n^2$ limit is shown for reference (black dashed lines).

becomes less relevant with respect to the antireflection effect. The dash-dotted lines in Fig. 3(a) represent the photocurrents achieved in the case of an infinitely long carrier diffusion length (i.e., when all the photogenerated carriers are extracted from the cell). As can be noted, these photocurrents diverge from the actual photocurrents (solid lines) only for cell thicknesses above 50 $\mu$m, i.e., for thicknesses comparable with the minority carrier diffusion length. The graph of Fig. 3(a) also shows that the photocurrents achieved with a Mie coating are roughly halfway between those achieved with a standard flat coating, and those achieved in the $4n^2$ light-trapping limit. Similar results are observed in case of high surface recombination velocity $S$ [see Fig. 3(d)] and short bulk lifetime [see Fig. 3(g)]. In both cases, the photocurrent for cells thicker than 20 $\mu$m is reduced compared to the case in Fig. 3(a) due to reduced carrier collection for large cell thickness.

Fig. 3(b), (e), and (h) shows that for cells with Mie coating, $V_{\rm OC}$ is always higher than for a flat cell with a standard $Si_3N_4$ coating. This is a direct consequence of the higher photocurrent for the Mie-coated cell, as seen in Fig. 3(a), (d), and (g). For the Mie-coated cell with low surface and bulk recombination rates [see Fig. 3(b)] $V_{\rm OC}$ increases for decreasing cell thickness. This is due to the reduced effect of bulk recombination as the cell thickness decreases. For larger surface recombination velocities [see Fig. 3(e)], $V_{\rm OC}$ decreases with decreasing thickness, as surface recombination then dominates over bulk recombination. In this case, an optimum $V_{\rm OC}$ is found for a thickness of 10 $\mu$m for the cell with Mie coating and 20 $\mu$m for the cell with standard $Si_3N_4$ coating. For cells with strong bulk recombination [see Fig. 3(h)], a lower $V_{\rm OC}$ is observed for all thicknesses. However, in this case, the effect is stronger for thicker cells, where the bulk material quality plays a more important role due to the larger bulk volume.

Finally, Fig. 3(c), (f), and (i) shows a strong efficiency enhancement for Mie-coated cells. This is a direct consequence of the photocurrent enhancement due to the antireflection and light-trapping effects provided by the Mie scatterers and the enhanced voltage. In particular, for a 20-$\mu$m-thick cell with low bulk and surface recombination rates, an efficiency as high as 21.5% can be achieved, compared with an efficiency of 17.5% for a flat cell. For reference, a cell operating in the $4n^2$ light-trapping limit would yield an efficiency of 25.3%. The importance of the result for the Mie light-trapping coating relies in the fact that standard random textures commonly used for wafer-based c-Si solar cells cannot be applied to 20-$\mu$m-thick cells, as the feature size is comparable to the thickness of the cell. Recently, random nanotextures have been successfully applied to thin Si solar cells [3]. A first comparison of our theoretical modeling with the experimental results in [3] suggests that the Mie coating yields better light trapping than a random nanotexture, as

suggested by the larger value of $J_{\rm SC}$. However, a full comparison between Mie coatings and random textures requires further investigations. Fig. 3(c) also shows that a 5-$\mu$m-thick cell with Mie scatterers yields the same efficiency as a flat 100-$\mu$m-thick cell with standard $Si_3N_4$ coating. The Mie scatterers thus allow reducing the cell thickness by a factor of 20, maintaining the same power conversion efficiency. Similar results are observed for high surface recombination velocities $S$ [see Fig. 3(f)] and bulk lifetimes [see Fig. 3(i)]. In both cases, lower efficiencies are observed than for the cells with lower recombination rates due the lower photocurrents and voltages.

It is interesting to compare the results of Fig. 3 with the most recent experimental results achieved for high-efficiency heterojunction-with-intrinsic-thin-layer (HIT) solar cells. The table below reports the performance of a record-efficiency 98-$\mu$m-thick HIT solar cell realized by Panasonic-Sanyo [26] and that of the modeled 100-$\mu$m-thick cell, assuming $\tau_{\rm SRH} = 1$ ms and $S = 10$ cm/s in the $4n^2$ limit [black lines in Fig. 3(a)–(c)].

| Cell | Modeled 100 μm $4n^2$ limit | Panasonic-Sanyo HIT |
|---|---|---|
| $J_{SC}$ (mA/cm$^2$) | 38.9 | 39.5 |
| $V_{OC}$ (mV) | 730 | 750 |
| Fill Factor (%) | 85.1 | 83.2 |
| Efficiency (%) | 24.2 | 24.7 |

The table shows that our modeled best cell shows lower $J_{\rm SC}$ and $V_{\rm OC}$ than the Panasonic-Sanyo HIT cell. This might seem surprising, as the experimental HIT cell is understandably less "optimal" than our modeled cell. However, the values we obtain in our model depend on several parameters (doping lever, SRV, $\tau_{\rm SRH}$) that are different in our model with respect to the experimental HIT cell. On the other hand, our model assumes an ideal diode and, thus, yields a higher fill-factor than that of the HIT cell, which is limited by resistive losses in the a-Si and ITO layers. Overall, the efficiency of our best cell is in good agreement with that of the Panasonic-Sanyo cell.

The efficiencies shown in Figs. 3(c), (f), and (i) do not take into account the increased surface area of the Si Mie coating with respect to a flat cell. The calculations were repeated by scaling the surface recombination velocity by the surface area enhancement factor, which for our geometry is $\sim$1.58. Only a minor reduction in efficiency was observed (for a 20-$\mu$m-thick cell the efficiency was reduced from 21.5% to 21.3%). Note that this efficiency reduction can be avoided by employing a $TiO_2$-based Mie coating that can be made on top of a flat, passivated solar cell [27].

Finally, note that the Si Mie coating geometry used in this study was optimized for light incoupling (i.e., for the antireflection effect), but not for light trapping in a thin Si slab. Further optimization of the Si NC geometry for each solar cell thickness may yield even higher efficiencies.

To further investigate the crucial role of the Shockley–Read–Hall lifetime $\tau_{\rm SRH}$ and of the surface recombination velocities $S$, Fig. 4 shows the calculated solar cell efficiency (color lines) as a function of $\tau_{\rm SRH}$ (vertical axis) and $S$ (horizontal axis) for (a) a 5-$\mu$m-thick cell and (b) a 20-$\mu$m-thick cell with an Si NC Mie coating. For (a) a 5-$\mu$m-thick cell, efficiencies range from 19.5% for $\tau_{\rm SRH} = 1$ ms and $S = 1$ cm/s, down to 15% for $\tau_{\rm SRH} = 1$ $\mu$s and $S = 1000$ cm/s. Similarly, for a 20-$\mu$m-thick cell (a), efficiencies range from 21.5% to 14%. A comparison of the two graphs shows that a 20-$\mu$m-thick cell is more sensitive to variations of $\tau_{\rm SRH}$ than a 5-$\mu$m-thick cell, due to the larger volume. Similarly, a 5-$\mu$m-thick cell is more sensitive to variations of $S$ than a 20-$\mu$m-thick cell, due to the larger surface-to-volume ratio.

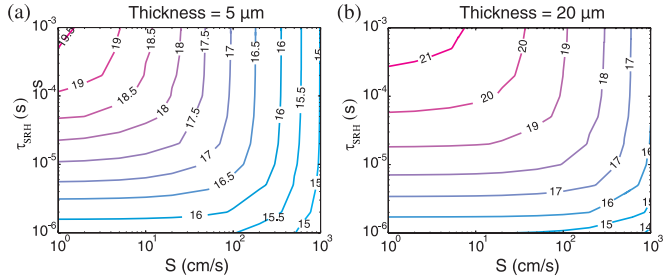


Fig. 4. Efficiency (colors) as a function of the Shockley–Read–Hall lifetime $\tau_{\rm SRH}$ (vertical axis) and the surface recombination velocity $S$, (a) for a 5-$\mu$m-thick cell and (b) a 20-$\mu$m-thick cell with Mie coating. The efficiency of a 5-$\mu$m-thick cell is more sensitive to variations in $S$, whereas the 20-$\mu$m-thick cell is more sensitive to variations in $\tau_{\rm SRH}$. For thin cells, efficiencies range from 19.5% to 15%; for the thick cell from 21.5% to 14%.

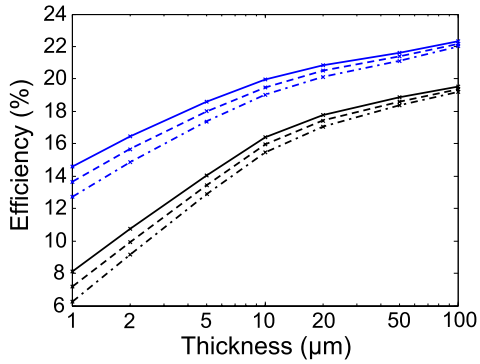


Fig. 5. Efficiency as a function of the solar cell thickness for a Si slab with the Mie coating (red) and with a standard $Si_3N_4$ coating (blue). Solid lines represent the case of a perfect back reflector, whereas dashed lines and dash–dotted lines are for a back reflector with 95% and 90% reflectivity, respectively. The efficiency of a 20-$\mu$m-thick cell is reduced by 1% (absolute) for a back reflector with 90% reflectivity.

In the analysis conducted so far, a perfect back reflector was considered. Simulations were also used for Si slabs with a back reflector with 95% and 90% reflectivity. These reflectivities correspond to the average reflectivity of a Si/Ag interface and to realistic reflectivities that can be achieved in c-Si solar cells [28], respectively. The nonperfect back reflector is implemented in the calculations by subtracting a constant factor from the total absorption spectrum. Note that this method does not consider the absorption in the metal due to coupling to surface plasmon polaritons at the Si/metal interface. Fig. 5 shows the calculated efficiency as a function of thickness, for a Si slab with a perfect back reflector (solid), and with a back reflector with 95% (dashed) and 90% (dot-dashed) reflectivity. Data are shown for an Si slab with flat $Si_3N_4$ coating (blue lines) and for an Si slab

with Mie coating (in red). Similarly to Fig. 3(c), we assume $\tau_{\mathrm{SRH}} = 1$ ms and $S = 10$ cm/s.

The graph shows a drop in efficiency of about 1% (absolute) for a 20-$\mu$m-thick cell with Mie coating when a back contact with 90% reflectivity is used instead of an ideal back reflector; the efficiency of the 20-$\mu$m-thick Mie-coated cell then drops to 20.5%. Similar losses are observed for cells with a standard $Si_3N_4$ coating.

## III. Conclusion

Using numerical simulations, we have shown that strongly reduced reflection and enhanced light trapping can be achieved in thin (1–100 $\mu$m) c-Si solar cells covered at the front surface with an array of Mie scattering Si NCs and coated with a $Si_3N_4$ anti-reflection layer. For thin Si slabs, near-infrared light trapping due to preferential scattering of light by the Mie scatterers into guided modes of the Si slab is directly observed from spectral peaks in the photocurrent. A strong increase in photocurrent is observed due to the Mie scatterers for all thicknesses in the range 1–20 $\mu$m. For thin cells, a strong increase in an open-circuit voltage is observed. For cells with low bulk and surface recombination ($\tau_{\mathrm{SRH}} = 1$ ms and $S = 10$ cm/s), a cell efficiency of 21.5% can be achieved for a 20-$\mu$m-thick Mie coated cell, compared with 17.5% for a flat cell. Silicon Mie scatterers are thus good candidates to substitute standard light-trapping techniques, such as pyramidal textures, that cannot be applied on thin solar cells. Our study opens new perspectives for designing high-efficiency thin-film c-Si solar cells.

## Acknowledgment

The authors would like to thank SARA Computing and Networking Services (www.sara.nl) for their support in using the Lisa Compute Cluster.

## References

[1] J. Dore, D. Ong, S. Varlamov, R. Egan, and M. A. Green, "Progress in laser-crystallised thin-film polycrystalline silicon solar cells," presented at the 39th IEEE Photovoltaic Spec. Conf., Tampa, FL, 2013.

[2] C. Becker, D. Amkreutz, T. Sontheimer, V. Preidel, D. Lockau, J. Haschke, L. Jogschies, C. Klimm, J. J. Merkel, P. Plocica, S. Steffens, and B. Rech, "Polycrystalline silicon thin-film solar cells: Status and perspectives," *Sol. Energy Mater. Sol. Cells*, vol. 119, pp. 112–123, 2013.

[3] S. Verlamov, J. Dore, R. Evans, D. Ong, B. Eggleston, O. Kunz, U. Schubert, T. Young, J. Huang, T. Soderstrom, K. Omaki, K. Kim, A. Teal, M. Jung, J. Yun, Z. M. Pakhuruddin, R. Egan, and M. A. Green, "Polycrystalline silicon on glass thin-film solar cells: A transition from solid-phase to liquid-phase crystallised silicon," *Sol. Energy Mater. Sol. Cells*, vol. 119, pp. 246–255, 2013.

[4] J. H. Petermann, D. Zielke, J. Schmidt, F. Haase, E. G. Rojas, and R. Brendel, "19%-efficient and 43 $\mu$m-thick crystalline Si solar cell from layer transfer using porous silicon," *Progress Photovoltaics. Res. Appl.*, vol. 20, pp. 1–5, 2012.

[5] F. Dross, K. Baert, T. Bearda, J. Deckers, V. Depauw, O. El Daif, I. Gordon, A. Gougam, J. Govaerts, S. Granata, R. Labie, X. Loozen, M. Martini, A. Masolin, B. O'Sullivan, Y. Qiu, J. Vaes, D. Van Gestel, J. Van Hoeymissen, A. Vanleenhove, K. Van Nieuwenhuysen, S. Venkatachalam, M. Meuris, and J. Poortmans, "Crystalline thin-foil silicon solar cells: where crystalline quality meets thin-film processing," *Progress Photovoltaics, Res. Appl.*, vol. 20, pp. 770–784, 2012.

[6] M. A. Green, *Solar Cells: Operating Principles, Technology and System Applications*. Englewood Cliffs, NJ: Prentice-Hall, 1998.

[7] W. H. Southwell, "Pyramid-array surface-relief structures producing antireflection index matching on optical surfaces," *J. Opt. Soc. Amer.*, vol. 8, pp. 549–553, 1991.

[8] H. A. Atwater and A. Polman, "Plasmonics for improved photovoltaic devices," *Nat. Mater.*, vol. 9, pp. 205–213, 2010.

[9] P. Spinelli, M. Hebbink, L. Black, F. O. Lenzmann, and A. Polman, "Optical impedance matching using coupled metal nanoparticle arrays," *Nano Lett*, vol. 11, pp. 1760–1765, 2011.

[10] K. R. Catchpole and A. Polman, "Design principles for particle plasmon enhanced solar cells," *Appl. Phys. Lett.*, vol. 93, pp. 191113-1–191113-3, 2008.

[11] D. Derkacs, S. H. Lim, P. Matheu, W. Mar, and E. T. Yu, "Improved performance of amorphous silicon solar cells via scattering from surface plasmon polaritons in nearby metallic nanoparticles," *Appl. Phys. Lett.*, vol. 89, pp. 93103-1–93103-3, 2006.

[12] S. Pillai, K. R. Catchpole, T. Trupke, and M. A. Green, "Surface plasmon enhanced silicon solar cells," *J. Appl. Phys.*, vol. 101, pp. 93105-1–93105-8, 2007.

[13] T. L. Temple, G. D. K. Mahanama, H. S. Reehal, and D. M. Bagnall, "Influence of localized surface plasmon excitation in silver nanoparticles on the performance of silicon solar cells," *Sol. Energy Mater. Sol. Cells*, vol. 93, pp. 1978–1985, 2009.

[14] P. Matheu, S. H. Lim, D. Derkacs, C. McPheeters, and E. T. Yu, "Metal and dielectric nanoparticle scattering for improved optical absorption in photovoltaic devices," *Appl. Phys. Lett.*, vol. 93, pp. 113108-1–113108-3, 2008.

[15] P. Spinelli, M. A. Verschuuren, and A. Polman, "Broadband omnidirectional antireflection coating using subwavelength surface Mie resonators," *Nat. Comm*, vol. 3, pp. 692-1–692-5, 2012.

[16] G. Mie, "Beitrage zur optik truber medien, speziell kolloidaler metallosungen," *Ann. Phys.*, vol. 330, pp. 377–445, 1908.

[17] T. Coenen, J. van de Groep, and A. Polman, "Resonant Mie modes of single silicon nanocavities excited by electron irradiation," *ACS Nano*, vol. 7, p. 1689—1698, 2013.

[18] *FDTD Solutions 8.0*, Lumerical Inc., Vancouver, BC, Canada, 2012.

[19] M. van Lare, F. Lenzmann, M. A. Verschuuren, and A. Polman, "Mode coupling by plasmonic surface scatterers in thin-film silicon solar cells," *Appl. Phys. Lett*, vol. 101, pp. 221110-1–221110-4, 2012.

[20] S. De Wolf, A. Descoeudres, Z. C. Holman, and C. Ballif, "High-efficiency silicon heterojunction solar cells: A review," *Green*, vol. 2, pp. 7–24, 2012.

[21] A. Luque and S. Hegedus, *Handbook of Photovoltaic Science and Engineering*. New York: Wiley, 2011.

[22] M. J. Kerr and A. Cuevas, "General parametrization of Auger recombination in crystalline silicon," *J. Appl. Phys.*, vol. 91, pp. 2473–2480, 2002.

[23] R. A. Sinton and A. Cuevas, "Contactless determination of current-voltage characteristic and minority carrier lifetimes in semiconductors from quasisteadystate photoconductance data," *Appl. Phys. Lett.*, vol. 69, pp. 2510–2512, 1996.

[24] E. Yablonovitch and G. D. Cody, "Intensity enhancement in textured optical sheets for solar cells," *IEEE Trans. Electron Devices*, vol. ED-29, no. 2, pp. 300–305, Feb. 1982.

[25] H. W. Deckman, C. B. Roxlo, and E. Yablonovitch, "Maximum statistical increase of optical absorption in textured semiconductor films," *Opt. Lett.*, vol. 8, pp. 491–493, 1983.

[26] M. Taguchi, A. Yano, S. Tohoda, and K. Matsuyama, "24.7% record efficiency HIT solar cell on thin silicon wafer," presented at the 39th IEEE Photovoltaic Spec. Conf., Tampa, FL, USA, 2013.

[27] P. Spinelli, B. Macco, M. A. Verschuuren, W. M. M. Kessels, and A. Polman, "$Al_2O_3/TiO_2$ nano-pattern antireflection coating with ultralow surface recombination," *Appl. Phys. Lett.*, vol. 102, 233902, 2013.

[28] R. Santbergen, J. M. Goud, M. Zeman, J. A. M. van Roosmalen, and R. J. C. van Zolingen, "The AM1.5 absorption factor of thin-film solar cells," *Solar Energy Mater. Solar Cells*, vol. 94, pp. 715–723, 2010.

Authors' photographs and biographies not available at the time of publication.